Rotating disk flow stability in electrochemical cells: Effect of the transport of a chemical species

N. Mangiavacchi[a)]
Department of Mechanical Engineering, GESAR Group, State University of Rio de Janeiro, R. São Francisco Xavier 524, 20550-013 Rio de Janeiro RJ, Brazil

J. Pontes[b)]
Department of Metallurgy and Materials Engineering, EP-COPPE, Federal University of Rio de Janeiro, P.O. Box 68505, 21941-972 Rio de Janeiro RJ, Brazil

O. E. Barcia[c)]
Institute of Chemistry, IQ, Federal University of Rio de Janeiro, P.O. Box 68505, 21941-972 Rio de Janeiro RJ, Brazil

O. R. Mattos[d)]
Department of Metallurgy and Materials Engineering, COPPE, Federal University of Rio de Janeiro, P.O. Box 68505, 21941-972 Rio de Janeiro RJ, Brazil

B. Tribollet[e)]
UPR15–CNRS, Laboratoire Interfaces et Systèmes Electrochimiques, 4 place Jussieu, 75252 Paris Cedex 05, France

(Received 26 June 2007; accepted 9 October 2007; published online 20 November 2007)

We consider the stability of rotating disk flow coupled, through the fluid viscosity, to the mass concentration field of a chemical species. This configuration refers to an electrochemical cell where the working electrode consists of an iron rotating rod, which is dissolved in the 1 M H_2SO_4 solution of the electrolyte. Polarization curves obtained in these cells present a current instability at the beginning of the region where the current is controlled by the mass transport. The instability appears at a certain value of the applied potential and is suppressed beyond another value. Dissolution of the electrode gives rise to a thin concentration boundary layer, due to a Schmidt number $Sc=2000$ of the setup. This boundary layer, together with the potential applied to the electrode, leads to an increase in the fluid viscosity and to a decrease in the diffusion coefficient, both affecting the chemical species field. Since the current is proportional to the normal derivative of the species concentration at the interface, an instability of the coupled fields at sufficiently low Reynolds numbers would result in a current instability. This work deals with the question of whether the coupling reduces the critical Reynolds number to values comparable to those attained in experimental setups, and if a possible field instability would be large enough to drive a detectable current instability. A phenomenological law is assumed, relating the fluid viscosity to the concentration of the chemical species. Parameters appearing in this law are evaluated on the basis of experimental electrochemical data. The steady-state solution is obtained by solving the coupled hydrodynamic and mass concentration equations. A temporal stability analysis is made, showing that small variations in the fluid viscosity significantly affect the stability of the flow. The analysis reveals the existence of a new unstable region, not found in the case of constant viscosity fluids. We call modes in this new unstable region *chemical modes*, in contrast with the *hydrodynamic modes*, which are amplified in the case of constant viscosity fluids. The chemical modes are destabilized at much lower Reynolds numbers than the hydrodynamic ones and close to values attained in electrochemical setups, in the most relevant cases. Hydrodynamic modes are strongly affected by the coupling in three aspects: the critical Reynolds number of this region is of order of 50% smaller than in the case of constant viscosity fluids, the unstable region is enlarged to a wider range of wave numbers, and the rate of growth of unstable modes is 30% larger for comparable Reynolds numbers. Concentration eigenmodes in the new unstable region show a combination of properties including rate of growth, amplitude higher than the amplitude of the hydrodynamic variables, and high normal derivative at the interface, sufficiently strong to drive detectable current oscillations. The destabilizing effect of a higher interface viscosity attains a maximum when the ratio between the interface and the bulk

[a)]Electronic mail: norberto.mangiavacchi@gmail.com.
[b)]Electronic mail: jopontes@metalmat.ufrj.br.
[c)]Electronic mail: barcia@metalmat.ufrj.br.
[d)]Electronic mail: omattos@metalmat.ufrj.br.
[e)]Electronic mail: bt@ccr.jussieu.fr.

viscosities, ν_0/ν_∞, takes a value close to 1.5. Below this value, as the viscosity stratification diminishes and the condition of uniform viscosity is restored, the unstable region of chemical modes moves to higher Reynolds and eventually disappears. Conversely, as the ratio ν_0/ν_∞ increases beyond the value 1.5, the new unstable region also collapses and the neutral curve of hydrodynamic modes tends to the one of constant viscosity fluids. A sustained increase of the interfacial viscosity and the high Schmidt number results in an *in facto* field discontinuity with a thin high viscosity layer at the interface and restored constant viscous hydrodynamic boundary layer. A link between the current instability and the stability of the coupled fields may be inferred from the present analysis. © *2007 American Institute of Physics*. [DOI: 10.1063/1.2805844]

I. INTRODUCTION

Electrochemical cells using a rotating disk electrode are a widely used experimental tool in electrochemistry, due to the simplicity of the setup and the fact that the mass flux is independent of the radial position along the disk, at steady-state conditions.[1] Furthermore, the rate of transfer of ions close to the electrode is conveniently controlled through the angular velocity imposed to the electrode. This rate of transfer defines the maximum steady-state current attained in an experiment. Polarization curves obtained in these cells present a current instability at the beginning of the region where the current is controlled by the mass transport. The instability appears at a certain value of the applied potential and is suppressed beyond another value.[3]

The existence of a hydrodynamic instability in rotating disk flow has been the object of a number of investigations, both experimental and theoretical in the case of fluids with uniform viscosity. The main result shows that the steady flow becomes unstable beyond a critical Reynolds number that measures a nondimensional distance from the disk axis.

A review of the literature on the subject is presented in a previous paper,[4] where the authors addressed the stability of rotating disk flow in electrochemical cells, in which the fluid viscosity varies along the axial direction, according to an imposed profile.

We also mention the existence of flow stability studies of electrical conducting fluids with variable conductivity,[14] and of fluids with a viscosity stratification, confined or not to a thin region.[13,15] These studies show that, in some cases, viscosity stratification acts as a stabilization factor, by limiting the transfer of energy from the mean flow to fluctuations, as shown by Govindarajan *et al.*[13] for a channel flow configuration.

In our previous paper,[4] we considered the problem of rotating disk flow stability in the presence of the stratified viscosity profile proposed by Barcia *et al.*,[2] but we did not take into account the coupling between the hydrodynamic and the mass concentration field of chemical species. The results indicate that the stability properties of the flow are strongly affected by the stationary stratified viscosity profile, leading to a broader range of unstable wave numbers. In the present paper, we go one step further, by considering the stability of the hydrodynamic field coupled to the transport of one relevant chemical species, originating from the dissolution of the iron electrode. Coupling appears through a concentration-dependent viscosity. Since the current is proportional to the normal derivative of the ion concentration at the electrode surface[2] (see Sec. III B), a reduction of the critical Reynolds number to typical values found in experimental conditions could lead to a current instability. Investigation of the stability properties of the coupled fields and of the existence of a possible link between the flow stability and the current oscillations is, thus, the main purpose of this paper. A phenomenological law is assumed, relating the fluid viscosity to the concentration of a representative chemical species, and the parameters of this law are estimated based on experimental electrochemical data.

In spite of the importance of absolute instabilities in the transition to turbulence, we restrict ourselves to the study of the neutral curve of stationary convective instabilities that represent the lowest limit below which no small disturbances are amplified.[5]

The paper is organized as follows. Section II describes the governing equations. Section III deals with the variable viscosity steady flow, which is the subject of the following stability analysis. Section IV deals with the linearized equations of the perturbed flow and discusses the results of the stability analysis. Section V summarizes the major questions addressed in this work. Details about the derivation of the steady-state solution and on the stability equations are given in Appendixes A and B, and a brief discussion of the numerical procedure for solving the stability problem is given in Appendix C.

II. GOVERNING EQUATIONS

The problem is governed by the continuity and the Navier-Stokes equations, coupled through the viscosity, to the transport equation of a relevant chemical species. These equations, written in the frame attached to the surface of the rotating disk, read

$$\operatorname{div} \mathbf{v} = 0, \tag{1}$$

$$\frac{D\mathbf{v}}{Dt} = -2\boldsymbol{\Omega} \times \mathbf{v} - \boldsymbol{\Omega} \times (\boldsymbol{\Omega} \times \mathbf{r}) - \frac{1}{\rho}\,\mathbf{grad}\, p + \frac{1}{\rho} \operatorname{div} \tau, \tag{2}$$

$$\frac{D\mathcal{C}}{Dt} = \operatorname{div}(\mathcal{D}\,\mathbf{grad}\,\mathcal{C}), \tag{3}$$

where $\boldsymbol{\Omega}$ is the angular velocity of the rotating disk electrode, $\mathcal{C}$ and $\mathcal{D}$ are, respectively, the concentration and the diffusion coefficient of a representative chemical species, and τ is the viscous stress tensor for a fluid with variable viscosity. Components of τ are given by[6]

$$\tau_{rr} = 2\mu \frac{\partial v_r}{\partial r}, \tag{4}$$

$$\tau_{\theta\theta} = 2\mu \left(\frac{1}{r} \frac{\partial v_\theta}{\partial \theta} + \frac{v_r}{r} \right), \tag{5}$$

$$\tau_{zz} = 2\mu \frac{\partial v_z}{\partial z}, \tag{6}$$

$$\tau_{r\theta} = \tau_{\theta r} = \mu \left[r \frac{\partial}{\partial r} \left(\frac{v_\theta}{r} \right) + \frac{1}{r} \frac{\partial v_r}{\partial \theta} \right], \tag{7}$$

$$\tau_{\theta z} = \tau_{z\theta} = \mu \left(\frac{\partial v_\theta}{\partial z} + \frac{1}{r} \frac{\partial v_z}{\partial \theta} \right), \tag{8}$$

$$\tau_{zr} = \tau_{rz} = \mu \left(\frac{\partial v_z}{\partial r} + \frac{\partial v_r}{\partial z} \right), \tag{9}$$

where μ is the dynamic viscosity of the fluid.

We rewrite the evolution equations in nondimensional form. Variables having units of length or its reciprocal (radial and axial coordinates, perturbation wavenumber along the radial direction) are made nondimensional with the length used to measure the thickness of the boundary layer, $(\nu_\infty/\Omega)^{1/2}$, where ν_∞ is the bulk viscosity of the fluid. Velocity components are divided by the local imposed azimuthal velocity $r_e\Omega$, pressure is divided by $\rho(r_e\Omega)^2$, viscosity is divided by the bulk viscosity, ν_∞, and time and the eigenvalue of the linearized problem are made nondimensional with the time required by a particle, turning with the azimuthal velocity $r_e\Omega$, to move a distance equal to the reference length, $(\nu_\infty/\Omega)^{1/2}$. Here, r_e is the dimensional coordinate along the radial direction at which the stability analysis is carried out. The nondimensional concentration of the chemical species is defined by

$$C = \frac{\mathcal{C} - \mathcal{C}_\infty}{\mathcal{C}_S - \mathcal{C}_\infty}, \tag{10}$$

where $\mathcal{C}_S$ and $\mathcal{C}_\infty$ are, respectively, the concentration of the chemical species at the electrode surface and in the bulk. We define also the Reynolds and the Schmidt numbers by the relations

$$R = r_e \left(\frac{\Omega}{\nu_\infty} \right)^{1/2} \quad \text{and} \quad \mathrm{Sc} = \frac{\mathcal{D}_\infty}{\nu_\infty}. \tag{11}$$

At this point, we assume that the viscosity depends on the nondimensional concentration of the chemical species according to

$$\nu = \nu_\infty \exp(mC), \tag{12}$$

where m is a nondimensional parameter depending on the electrochemical characteristics of the system (electrode material, type of electrolyte, applied potential), but not on the concentration of the chemical species. In particular, this parameter defines the interface viscosity, given by $\nu = \nu_\infty \exp(m)$. We also assume the Stokes-Einstein law, which postulates that the product of the diffusion coefficient by the viscosity is constant,

$$\mathcal{D}\nu = \mathcal{D}_\infty \nu_\infty, \tag{13}$$

where $\mathcal{D}_\infty$ is the bulk diffusion coefficient. Using the bulk coefficients to rewrite Eqs. (13) and (12) in nondimensional form, we obtain

$$\mathcal{D}\nu = 1 \quad \text{and} \quad \nu = \exp(mC). \tag{14}$$

Equations (1)–(3) are rewritten as follows, in nondimensional form,

$$\operatorname{div} \mathbf{v} = 0, \tag{15}$$

$$\frac{D\mathbf{v}}{Dt} = -2\mathbf{e}_z \times \mathbf{v} - \mathbf{e}_z \times (\mathbf{e}_z \times r\mathbf{e}_r) - \mathbf{grad}\, p + \frac{1}{R} \operatorname{div} \tau, \tag{16}$$

$$\frac{DC}{Dt} = \frac{1}{R\mathrm{Sc}} \operatorname{div}(\mathcal{D}\, \mathbf{grad}\, C). \tag{17}$$

A destabilizing potential of the coupling between the hydrodynamic and the chemical species fields can be seen in Eqs. (15)–(17): the Reynolds number in Eq. (17) is multiplied by the Schmidt number, which takes here the value Sc=2000, typical for electrochemical cells.

III. THE BASE STATE

A. Base state equations

The base state is the von Kármán similarity solution for a fluid with the viscosity depending on the concentration field, which is assumed to vary along the axial coordinate only,

$$\begin{pmatrix} \bar{v}_r \\ \bar{v}_\theta \\ \bar{v}_z \\ \bar{p} \\ \bar{\mathcal{C}} \end{pmatrix} = \begin{pmatrix} r\Omega F(z) \\ r\Omega G(z) \\ (\nu_\infty \Omega)^{1/2} H(z) \\ \rho \nu_\infty \Omega P(z) \\ \mathcal{C}_\infty + (\mathcal{C}_S - \mathcal{C}_\infty) C(z) \end{pmatrix}. \tag{18}$$

All variables in Eq. (18) are dimensional, except the axial dependent profiles, F, G, H, C, and the axial coordinate z. Boundary conditions for F, G, H, and P are $F=G=H=P=0$ at the disk surface ($z=0$), $F=H'=0$, and $G'=-1$ as $z \to \infty$. The nondimensional concentration profile, C, varies from 1 at $z=0$ to 0 as $z \to \infty$.

Introducing Eq. (18) and the constitutive equations of the stress tensor [Eqs. (4)–(9)] in Eqs. (1)–(3), together with Eqs. (12) and (13), we obtain the ordinary nonlinear system for the axial profiles F, G, H, P, and C,

$$2F + H' = 0, \tag{19}$$

$$F^2 - (G+1)^2 + HF' - \nu F'' - \nu' F' = 0, \tag{20}$$

$$2F(G+1) + HG' - \nu G'' - \nu' G' = 0, \tag{21}$$

$$P' + HH' - \nu H'' - 2\nu' H' = 0, \tag{22}$$

$$\mathrm{Sc}HC' - \frac{C''}{\nu} + \frac{\nu'}{\nu^2}C' = 0, \tag{23}$$

where the prime denotes derivatives with respect to the nondimensional axial coordinate z. The viscosity ν and its derivatives are written in nondimensional form in the above equations, and

$$\nu' = m\exp(mC)C'. \tag{24}$$

Details concerning the derivation of Eqs. (19)–(23) are given in Appendix A.

B. Evaluation of the viscosity at the electrode/electrolyte interface

Equations (19)–(23) are solved using the Newton method, in a staggered, uniform grid of points, with space derivatives represented by second-order approximations. Solving these equations requires specification of two parameters: the bulk Schmidt number and the parameter m appearing in Eq. (12), which ultimately defines the electrolyte viscosity at the interface with the electrode. Though both questions will be addressed in a separate paper by the authors, we briefly review the key points of the subject for the sake of completeness.

At this point, we assume that the limit current density at the interface is proportional to the concentration gradient of the relevant chemical species generated by the dissolution of the electrode. Ion migration due to the potential gradient is neglected. The current density is given by the relation[2]

$$\frac{i}{n\mathcal{F}\dfrac{1}{\mathrm{Sc}}\dfrac{1}{\nu_0/\nu_\infty}(\mathcal{C}_\infty - \mathcal{C}_s)\sqrt{\nu_\infty\Omega}} = \left.\frac{dC}{dz}\right|_{z=0}, \tag{25}$$

where i is expressed in $\mathrm{A/cm^2}$, n is the valence number of the chemical species ($n=2$), $\mathcal{F}=96500$ C/mol is the Faraday constant, $\mathcal{C}_s=2.0\times10^{-3}$ mol/cm^3 is the dimensional concentration of the species at the electrode interface (saturated condition), $\mathcal{C}_\infty=0$ mol/cm^3, and ν_0 is the fluid viscosity at the interface. The limit current density obtained experimentally is $i=0.8810$ A/cm^2 at 900 rpm (Ref. 3).

An initial value is specified for m, and Eqs. (19)–(23) are solved. The ratio ν_0/ν_∞ is evaluated and the nondimensional normal derivative of the concentration at the interface, $dC/dz|_{z=0}$, is obtained from the profiles. These figures are introduced in Eq. (25), leading to a value for the current density. The value initially specified for m is corrected and the procedure is repeated until convergence to the experimental value of i is reached. At convergence, we obtain $\nu_0/\nu_\infty=2.255$ ($m=\ln\nu/\nu_\infty$).

C. Base state profiles

The high Schmidt number leads to a concentration boundary layer much thinner than the hydrodynamic one. An estimation of the ratio between the thicknesses of the hydrodynamic (δ_h) and the concentration (δ_c) boundary layers can be made by using the following relation, proposed by Levich:[1]

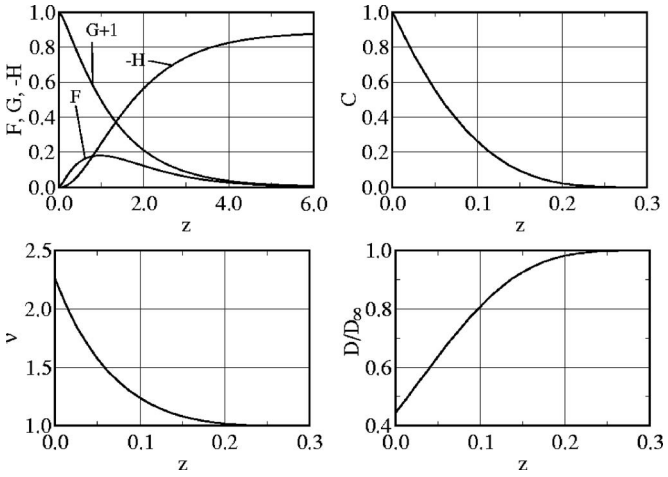

FIG. 1. Stationary dimensionless velocity, concentration, viscosity, and diffusion profiles, F, G, H, and C for $\nu_0/\nu_\infty=2.255$ and $\mathrm{Sc}=2000$.

$$\frac{\delta_h}{\delta_c} \approx 2\mathrm{Sc}^{1/3}. \tag{26}$$

The nondimensional velocity, concentration, viscosity, and diffusion coefficient profiles, F, G, H, C, ν, and $\mathcal{D}$, obtained for $\nu_0/\nu_\infty=2.255$ and $\mathrm{Sc}=2000$, are shown in Fig. 1. Upon assuming $\delta_h=6$ for the hydrodynamic boundary layer, we estimate $\delta_c=0.24$ using Eq. (26). The profiles numerically obtained agree with this estimate.

The thin concentration boundary layer results in velocity profiles very close to the ones obtained for the constant viscosity case. In particular, we obtain $H=-0.88559$ far from the disk for the variable viscosity flow considered, a figure slightly different from the asymptotic value for the constant viscosity case, $H=-0.88447$. However, the derivatives of the velocity profiles are strongly affected inside the concentration boundary layer, as shown in Fig. 2.

IV. STABILITY OF THE BASE STATE

A. Stability equations

We turn now to the question of the stability of the base state with respect to small disturbances. The hydrodynamic and chemical fields are written as a sum of the base state plus a perturbation,

$$\begin{aligned} &v_r = \bar{v}_r + \tilde{v}_r, \quad v_\theta = \bar{v}_\theta + \tilde{v}_\theta, \quad v_z = \bar{v}_r + \tilde{v}_z, \\ &p = \bar{p} + \tilde{p}, \quad \mathcal{C}_T = \bar{\mathcal{C}} + \tilde{\mathcal{C}}, \end{aligned} \tag{27}$$

where the perturbation, in dimensional form, is given by

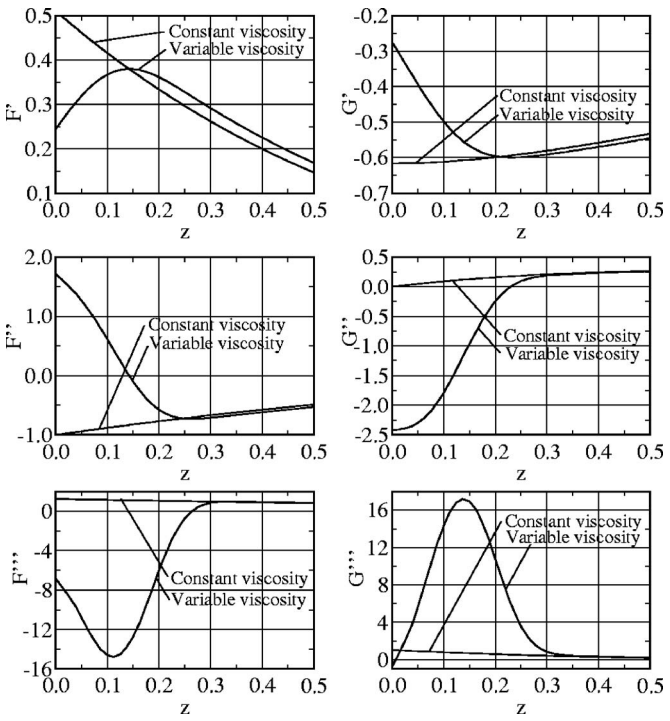

FIG. 2. The first three derivatives of the nondimensional velocity profiles, F and G, for the constant and variable viscosity cases, with $\nu_0/\nu_\infty=2.255$ and $\mathrm{Sc}=2000$.

$$\begin{pmatrix} \tilde{v}_r \\ \tilde{v}_\theta \\ \tilde{v}_z \\ \tilde{p} \\ \tilde{C} \end{pmatrix} = \begin{pmatrix} r_e\Omega f \\ r_e\Omega g \\ r_e\Omega h \\ \rho\nu_\infty\Omega\pi \\ (C_s - C_\infty)c \end{pmatrix} \exp[i(\alpha r + \beta R\theta - \omega t)] + \text{c.c.} \tag{28}$$

Here ω is a complex number, with $\Re(\omega)$ and $\Im(\omega)$ being, respectively, the frequency and the rate of growth of the perturbation. The functions f, g, h, π, and c depend on the axial coordinate z, and the parameters α and β are the components of the perturbation wave vector along the radial and azimuthal directions. For a given time, the phase of the perturbation is constant along branches of a logarithmic spiral, with the branches curved in the clockwise direction if β/α is positive and counterclockwise if it is negative. The structure turns counterclockwise if $\Re(\omega)/\beta$ is positive and clockwise if it is negative.

The base and the perturbation, given by Eqs. (18) and (28), are rewritten in nondimensional form,

$$\begin{pmatrix} \bar{v}_r \\ \bar{v}_\theta \\ \bar{v}_z \\ \bar{p} \\ \bar{C} \end{pmatrix} = \begin{pmatrix} rF/R \\ rG/R \\ H/R \\ p/R^2 \\ C \end{pmatrix}, \tag{29}$$

$$\begin{pmatrix} \tilde{v}_r \\ \tilde{v}_\theta \\ \tilde{v}_z \\ \tilde{p} \\ \tilde{c} \end{pmatrix} = \begin{pmatrix} f \\ g \\ h \\ \pi \\ c \end{pmatrix} \exp[i(\alpha r + \beta R\theta - \omega t)] + \text{c.c.} \tag{30}$$

The base state and the perturbation variables are introduced in Eqs. (15)–(17) and nonlinear terms are dropped. Perturbation variables are not, strictly speaking, separable since the resulting equations for the profiles f, g, h, π, and c still contain the radial coordinate r. In order to overcome the problem, it is necessary to make the *parallel flow* assumption, where it is assumed that variations of the above profiles are small as far as $\Delta r/r \ll 1$. This approximation holds whenever the stability analysis is carried sufficiently far from $r=0$. If variations of the profiles with r are small, this coordinate can be assumed as constant. The nondimensional constant r is the Reynolds number at which the stability analysis is carried. This is the parallel flow hypothesis. Adoption of this hypothesis in rotating disk flow[8–10] is made by replacing r by R.

To conclude, terms of order R^{-2} are dropped, leading to a generalized complex nonsymmetric eigenvalue-eigenfunction problem in the form

$$\begin{pmatrix} A_{11} & A_{12} & A_{13} \\ A_{21} & A_{22} & A_{23} \\ A_{31} & & A_{33} \end{pmatrix} \begin{pmatrix} h \\ \eta \\ c \end{pmatrix} = \omega R \begin{pmatrix} B_{11} & & \\ & B_{22} & \\ & & B_{33} \end{pmatrix} \begin{pmatrix} h \\ \eta \\ c \end{pmatrix}, \tag{31}$$

where $\eta=\alpha g-\beta f$, missing elements in the matrices are zero, and the operators A_{ij} and B_{ij} are given by

$$A_{11} = a_{114}D^4 + a_{113}D^3 + a_{112}D^2 + a_{111}D + a_{110},$$

$$A_{12} = a_{121}D + a_{120},$$

$$A_{13} = a_{132}D^2 + a_{131}D + a_{130},$$

$$A_{21} = a_{211}D + a_{210},$$

$$A_{22} = a_{222}D^2 + a_{221}D + a_{220},$$

$$A_{23} = a_{231}D + a_{230},$$

$$A_{31} = a_{310},$$

$$A_{33} = a_{332}D^2 + a_{331}D + a_{330},$$

$$B_{11} = D^2 - \bar{\lambda}^2,$$

$$B_{22} = 1,$$

$$B_{33} = i\mathrm{Sc},$$

with $D^n=d^n/dz^n$ and $\lambda^2=\alpha^2+\beta^2$. By defining $\bar{\alpha}=\alpha-i/R$ and $\bar{\lambda}^2=\alpha\bar{\alpha}+\beta^2$, we obtain for the coefficients a_{ijk},

$$a_{114} = i\nu,$$

$$a_{113} = i(2\nu' - H),$$

$$a_{112} = i\nu'' - i\nu(\lambda^2 + \bar{\lambda}^2) + R(\alpha F + \beta G) - i(H' + F),$$

$$a_{111} = -i\nu'(\lambda^2 + \bar{\lambda}^2) + iH\bar{\lambda}^2,$$

$$a_{110} = i\bar{\lambda}^2(\nu'' + \nu\lambda^2) - R(\alpha F + \beta G)\bar{\lambda}^2 - R(\bar{\alpha}F'' + \beta G'') + iH'\bar{\lambda}^2,$$

$$a_{121} = 2(G + 1),$$

$$a_{120} = 2G',$$

$$a_{132} = R(\bar{\alpha}F' + \beta G')\gamma,$$

$$a_{131} = [2R(\bar{\alpha}F'' + \beta G'') + 6i\bar{\lambda}^2 F]\gamma + 2R(\bar{\alpha}F' + \beta G')\gamma',$$

$$a_{130} = [R\bar{\lambda}^2(\alpha F' + \beta G') + R(\bar{\alpha}F''' + \beta G''') + 4i\bar{\lambda}^2 F']\gamma + [2R(\bar{\alpha}F'' + \beta G'') + 6i\bar{\lambda}^2 F]\gamma' + R(\bar{\alpha}F' + \beta G')\gamma'',$$

$$a_{211} = 2(G + 1),$$

$$a_{210} = -iR(\alpha G' - \beta F'),$$

$$a_{222} = i\nu,$$

$$a_{221} = i(\nu' - H),$$

$$a_{220} = -i\nu\lambda^2 + R(\alpha F + \beta G) - iF,$$

$$a_{231} = iR(\alpha G' - \beta F')\gamma,$$

$$a_{230} = iR[(\alpha G'' - \beta F'')\gamma + (\alpha G' - \beta F')\gamma'],$$

$$a_{310} = R\mathrm{Sc}C',$$

$$a_{332} = -\frac{1}{\bar{\nu}},$$

$$a_{331} = \frac{1}{\bar{\nu}}\left(\frac{\bar{\nu}'}{\bar{\nu}} + \frac{1}{\bar{\nu}}C'\gamma + \mathrm{Sc}\bar{\nu}H\right),$$

$$a_{330} = iR\mathrm{Sc}(\alpha F + \beta G) - \frac{1}{\bar{\nu}}\left\{-\bar{\lambda}^2 + \frac{1}{\bar{\nu}}\left[\left(2\frac{\bar{\nu}'}{\bar{\nu}}\gamma - \gamma'\right)C' - \gamma C''\right]\right\},$$

where $\gamma = d\nu/dC$. Details about the derivation of the above stability equations are given in Appendix B.

Equation (31) reduces to the linear stability equations derived by Malik[7] for rotating disk flow with constant viscosity fluids.

Boundary conditions of the problem require nonslip flow, vanishing axial component of the velocity, and saturation concentration of the chemical species at the electrode surface. These conditions are already fulfilled by the base state, so the hydrodynamic field cannot be modified by the perturbation at the electrode surface. As a consequence, we must require $h = \eta = c = 0$ in $z = 0$. Moreover, we conclude from Eq. (B6) that $h' = 0$ at the electrode surface. In $z \to \infty$, we require that the perturbation vanishes ($h = h' = \eta = c = 0$).

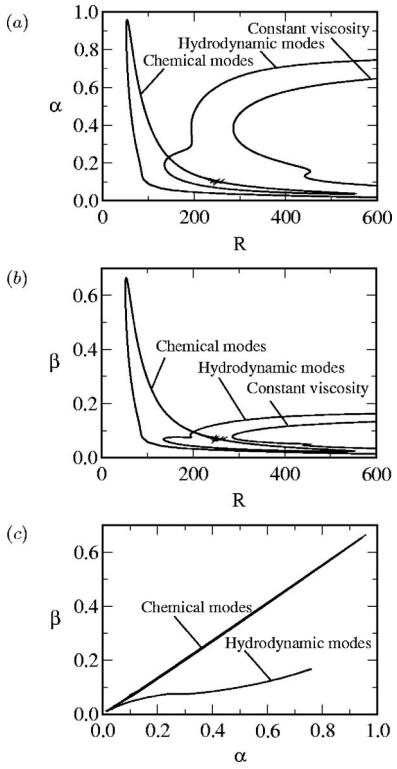

FIG. 3. The neutral stability curves of stationary perturbations [$\Re(\omega) = 0$] in the $R \times \alpha$ (a), $R \times \beta$ (b), and $\alpha \times \beta$ (c) planes.

B. Stationary neutral curves

The neutral stability curves for stationary disturbances [$\Re(\omega) = 0$], obtained by solving the eigenvalue-eigenfunction problem for $\mathrm{Sc} = 2000$ and $\nu_0/\nu_\infty = 2.255$, are presented in Fig. 3. Figures 3(a) and 3(b) show the neutral curves associated with the constant and the variable viscosity cases, in the $R \times \alpha$ and $R \times \beta$ plane, respectively. Figure 3(c) shows the curves of the variable viscosity case, in the $\alpha \times \beta$ plane. This figure shows that the coupling of the mass concentration to the hydrodynamic field affects the stability properties of the coupled fields by enlarging the unstable region to a wider range of wavenumbers and to a critical Reynolds number of order of 50% of the critical wavenumber of constant viscosity fluids.

Figure 3 shows also the existence of a new family of much more unstable modes. We refer to these new modes as *chemical* and to modes belonging to the former family as *hydrodynamic*.

The neutral curve for constant viscosity fluids presents two minima, the second one occurring at $R \approx 440$ and being associated with a second unstable mode, with a different profile from the one associated with the most unstable mode. This second mode is more affected by the variable viscosity field and becomes the most unstable hydrodynamic mode, in the variable viscosity case.

However, the new critical Reynolds number is now as-

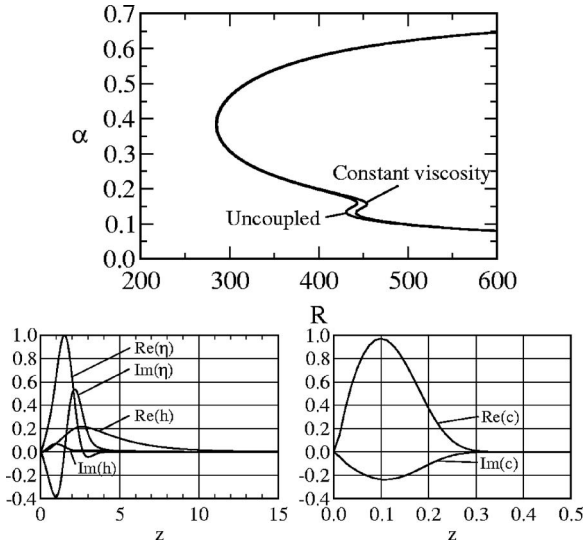

FIG. 4. Effect of decoupling the hydrodynamic equations [the first two rows of Eq. (31)] from the concentration transport equation: the figure shows, in the first row, the neutral stability curves for constant viscosity fluids and for a fluid with the steady viscosity profile shown in Fig. 1. The curves are practically identical, except close to the lower minimum. The second row shows a plot of an eigenmode at the point $R=285.39$, $\alpha=0.3857$, and $\beta=0.07774$, with the real and imaginary parts of h on the left and c on the right. The new unstable region of chemical modes no longer exists.

sociated with modes in the border of the unstable region of chemical modes. The critical Reynolds number for stationary disturbances is $R=52.3$, a number significantly smaller than 285.36, the critical value for constant viscosity fluids.[7]

We point out that the critical Reynolds number obtained is within the range of values attained in the experimental setup by Geraldo.[3] For instance, at 900 rpm, the Reynolds number based on the external radius of the electrode insulation ($r=5\times10^{-3}$ m and $\nu_\infty=1\times10^{-6}$ m^2 s^{-1}) is 48.54.

C. Effect of decoupling the hydrodynamic stability equations from the concentration transport equation

It is well known that the existence of inflection on the mean velocity profile are necessary and sufficient to destabilize inviscid flows.[11] In viscous cases, the flow usually becomes more stable as the velocity profile moves away from having an inflection point. Figure 2 shows that the second derivatives of the base state, F'' and G'', change signal inside the thin concentration boundary layer, indicating that an inflection on the velocity profiles actually occurs in the coupled case. The same inflection does not exist in the case of constant viscosity.

In order to verify the role played by the inflection and by the new terms added to the linear hydrodynamic stability equations [the first two rows of Eq. (31)], we perform a numerical experiment, consisting of setting operators $A_{13}=A_{23}=0$ in Eq. (31). In other words, we consider a fluid with a stationary viscosity stratification in a thin layer. The result is shown in Fig. 4. The first row presents the neutral curve obtained with the decoupling, together with the neutral curve of constant viscosity fluids. The second row shows a plot of an eigenmode on the neutral curve, close to the curve minimum. The neutral curves are almost identical, except close to the second minimum, showing that the coupling, and not the inflection on the base state profiles, is responsible for the enlargement of the unstable region. The stability properties are basically the ones of constant viscosity fluids, and this fact justifies the term *hydrodynamic region of unstable modes* that we use for the first unstable region. However, unstable eigenmodes in this region contain a concentration component c, driven by h and η, and the amplitude of this component is of the same order of the amplitude of the hydrodynamic variables, as shown in Fig. 4. The concentration component remains confined to a thin layer with thickness $\delta\approx0.3$. In addition, the second unstable region no longer exists.

We mention that Chikkadi *et al.*[12] arrived at similar results by showing that channel flow stability of fluids with a viscosity stratification is very little affected when compared to the stability properties of constant viscosity fluids.

D. Growth rate of unstable perturbations

The enlarged unstable hydrodynamic region suggests that modes inside this region might possibly have larger growth rates (ω_i) than unstable modes of constant viscosity fluids. Similarly, we could expect that the narrow region of unstable chemical modes could not allow for the existence of modes with large growth rates. This is the case, indeed. Figure 5 shows neutral and level curves evaluated for positive rates of growth for fluids with constant viscosity (a) and for the unstable region of hydrodynamic and chemical modes [(b) and (c), respectively].

An analysis of Fig. 5 shows that growth rates of chemical modes are more than one order of magnitude smaller than those of hydrodynamic modes. Growth rates are particularly small close to the electrode axis. As the point of analysis moves to larger distances from the electrode axis, the unstable region of chemical modes becomes narrower and limited to small wavenumbers, but higher growth rates are found. Nevertheless, the growth rates of chemical modes stay always one order of magnitude smaller than the one of hydrodynamic modes. Finally, a comparison between the growth rates of hydrodynamic and constant viscosity unstable modes [(a) and (b)] shows an increase of order of 30% in the former.

E. Marginally stable eigenmodes and flow streamlines

We address now the question of whether unstable chemical modes with critical Reynolds numbers on the order of 60 and growth rates 20 times smaller than typical unstable hydrodynamic modes could give raise to detectable current oscillations.

In order to answer the question, we mention that the amplitude of instabilities emerging from a Hopf bifurcation increases with the instability growth rate. Weakly nonlinear theory shows that the amplitude of unstable modes associated with complex eigenvalues saturates at levels proportional to the square root of the growth rate.[17] A second factor affecting the amplitude of the current instability is the rela-

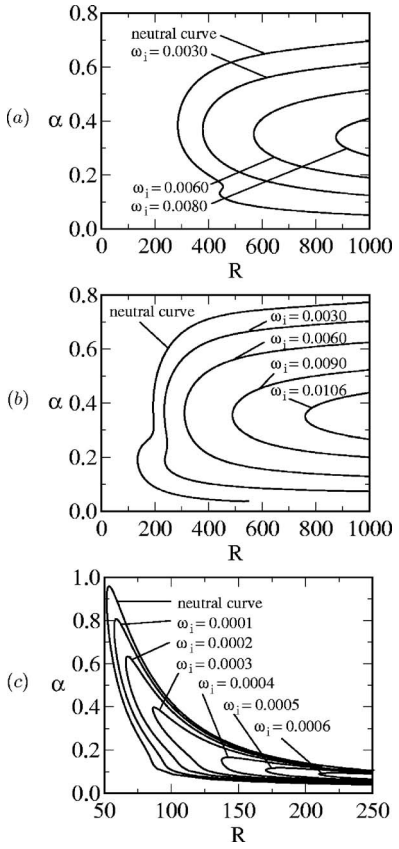

FIG. 5. Neutral and level curves with positive growth rates (ω_i) of fluids with constant viscosity (a) in the unstable region of hydrodynamic (b) and chemical modes (c) of the coupled case, in the $R\times\alpha$ planes. Similar curves are obtained in the $R\times\beta$ plane. The lower branch of the neutral curve of hydrodynamic modes, shown in (b), is drawn up to the border of the region of unstable chemical modes.

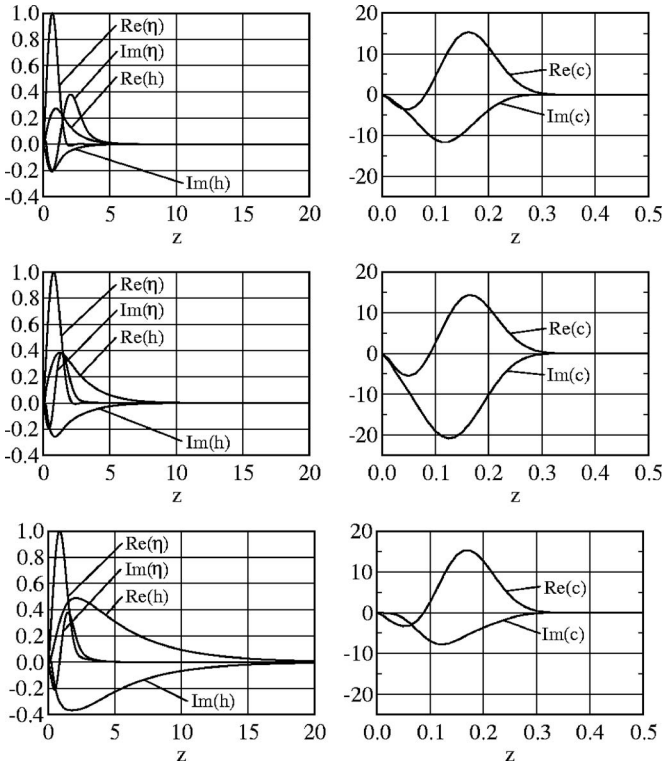

FIG. 6. Real and imaginary parts of three modes on the neutral curve of the chemical region, at the points $R=64.369$, $\alpha=0.81250$, $\beta=0.56278$ (first row), $R=60.394$, $\alpha=0.5000$, and $\beta=0.33949$ (second row), and $R=156.99$, $\alpha=0.20124$, and $\beta=0.13767$ (third row). The profiles show that modes in the upper and in the lower part of the neutral curve are similar. The eigenfunction is dominated by the chemical component c, which attains values more than 20 times larger than those associated with the hydrodynamic variables h and η. The chemical component c is confined to a thin layer close to the interface, leading to short-range variations and to high values of $dc/dz|_{z=0}$.

tive amplitude of the concentration component c of the eigenmodes, with respect to the amplitude of the hydrodynamic components, h and η. A third factor is the value of $dc/dz|_{z=0}$.

Figure 6 shows marginally stable modes on three points at the neutral curve of the chemical region. An analysis of Fig. 6 leads to the following conclusions:

(1) The amplitude of the c component of the modes in the chemical region is always 10 to 20 times larger than the amplitude of h and η. The eigenfunction is dominated by the chemical component c.
(2) The chemical component c stays confined to a thin layer with thickness $\delta_c\approx 0.3$, a characteristic length 20 times smaller than the length scale of the hydrodynamic variables h and η. Since $dc/dz|_{z=0}$ is of the order of δ_c^{-1}, very high values of this derivative are expected.
(3) The modes are qualitatively the same throughout the unstable chemical region.

Summing up, the low growth rate of the perturbation is balanced by the high value taken by the chemical component c and by its normal derivative at the electrode surface. The modes in the new region are dominated by the concentration component of the eigenfunction, justifying thus the term *chemical modes*. These facts indicate that the concentration fluctuations in the chemical region are sufficiently large to drive the current instability found in experimental conditions.

Figure 6 shows a progressive increase in the length of the h component of the modes, as α and β increase. The effect is explained by continuity reasons: a reduction in α and β requires a reduction in h' [see Eq. (B11)].

Figure 7 shows a reconstruction of the local streamlines of perturbation variables, with a plot of the (v_r,v_z) vector and level curves of the concentration at the same point in the $R\times z$ plane [(a)] and of (v_θ,v_z) in the $\theta\times z$ plane [(b)].

Figure 8 shows marginally stable modes at the two minima of the neutral curve of hydrodynamic modes. The chemical component of the eigenmode is, in both cases, confined to a thin boundary layer with a thickness $\delta_c\approx 0.3$. The modes are qualitatively different. The amplitude of the chemical component c is smaller than the amplitude of the hydrodynamic variables at the upper minimum and comparable to h and η at the lower minimum. The increase in the length of h is also observed, as α and β decrease. A plot of the local streamlines of perturbation variables, showing the (v_r,v_z) vector and level curves of the concentration in the $R\times z$ plane and of (v_θ,v_z) in the $\theta\times z$ plane are shown in Fig. 9 [(a) and (b), respectively].

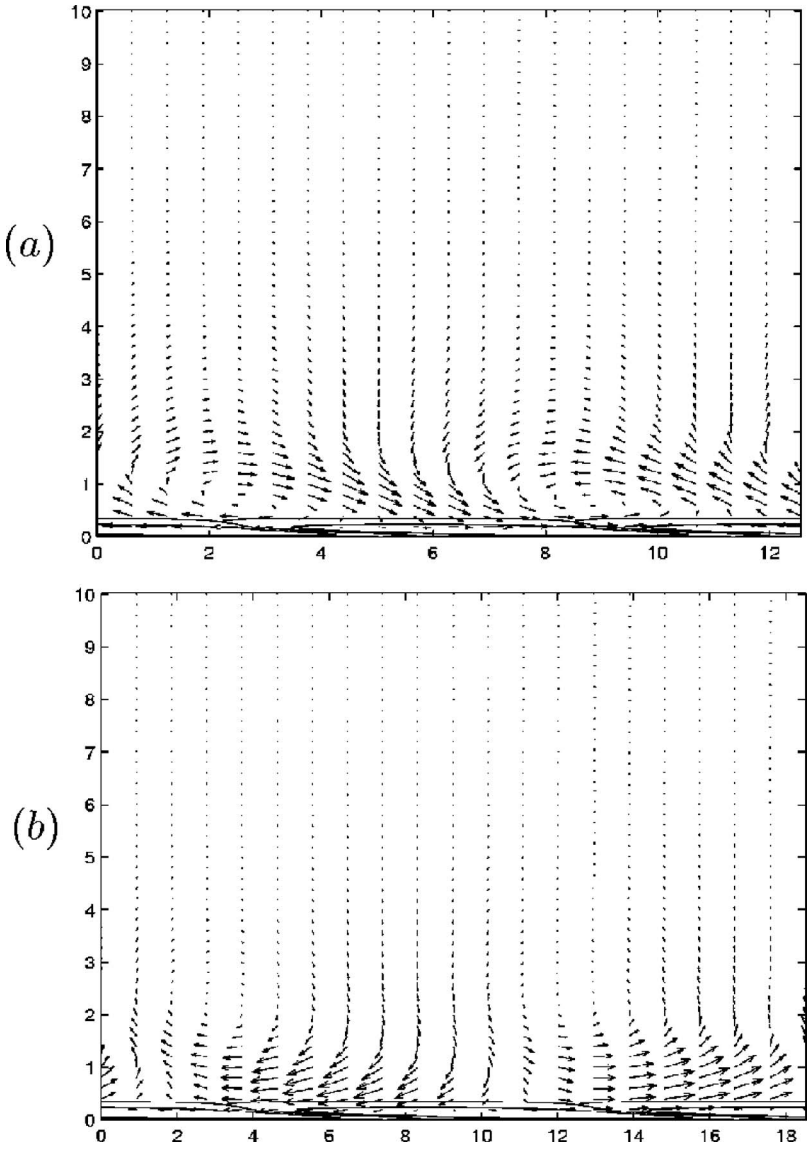

FIG. 7. Reconstruction of the local streamlines at the point $R=60.394$, $\alpha=0.5000$, and $\beta=0.33949$, located on the inner branch of the neutral curve of chemical modes. The figure shows a plot of the (v_r, v_z) vector in the $R\times z$ plane (a) and a plot of (v_θ, v_z) in the $\theta\times z$ plane (b). Two level curves of the concentration mode c are also shown in the lower part of (a) and (b).

F. Restoration of the stability properties of constant viscosity electrolytes as $\nu_0/\nu_\infty \to 1$

In this section, we study the effect of reducing the ratio ν_0/ν_∞ on the neutral curve, a situation that occurs when the potential applied to the cell is reduced. The results are shown in Fig. 10. The assumed Schmidt number is Sc=2000. Several conclusions can be taken from these curves:

(1) The case with $\nu_0/\nu_\infty=2.255$ is not the most unstable one. Cases with $\nu_0/\nu_\infty=1.8$ and 1.5 show a larger new region of chemical modes, with a critical Reynolds number very close to the one associated to the case with $\nu_0/\nu_\infty=2.255$. In addition, the range of unstable modes extends to higher values of α and β.
(2) As the value ν_0/ν_∞ is successively reduced to 1.8 and to 1.5, the new region shows a second minimum of unstable modes in the lower part. At $\nu_0/\nu_\infty=1.1$, the region of the lower minimum detaches from the new region and joins the unstable region of hydrodynamic modes. The absolute minimum of the neutral curves is located in this last region for $\nu_0/\nu_\infty=1.1$ and lower.
(3) By further reducing the ν_0/ν_∞, we observe that the new

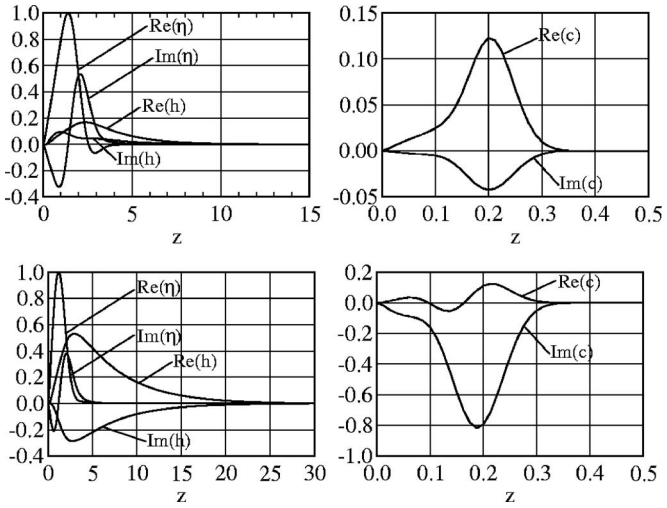

FIG. 8. Real and imaginary parts of modes at approximately the upper and the lower minimum of the neutral curve of the hydrodynamic region. First line: $R=208.77$, $\alpha=0.50869$, $\beta=0.10206$; second line: $R=135.48$, $\alpha=0.18726$, $\beta=0.067182$. The profiles confirm that modes in the upper part of the neutral curve are different from modes in the lower part. The chemical component c of the modes is confined to a thin layer, and the amplitudes of c, h, and η are of the same order.

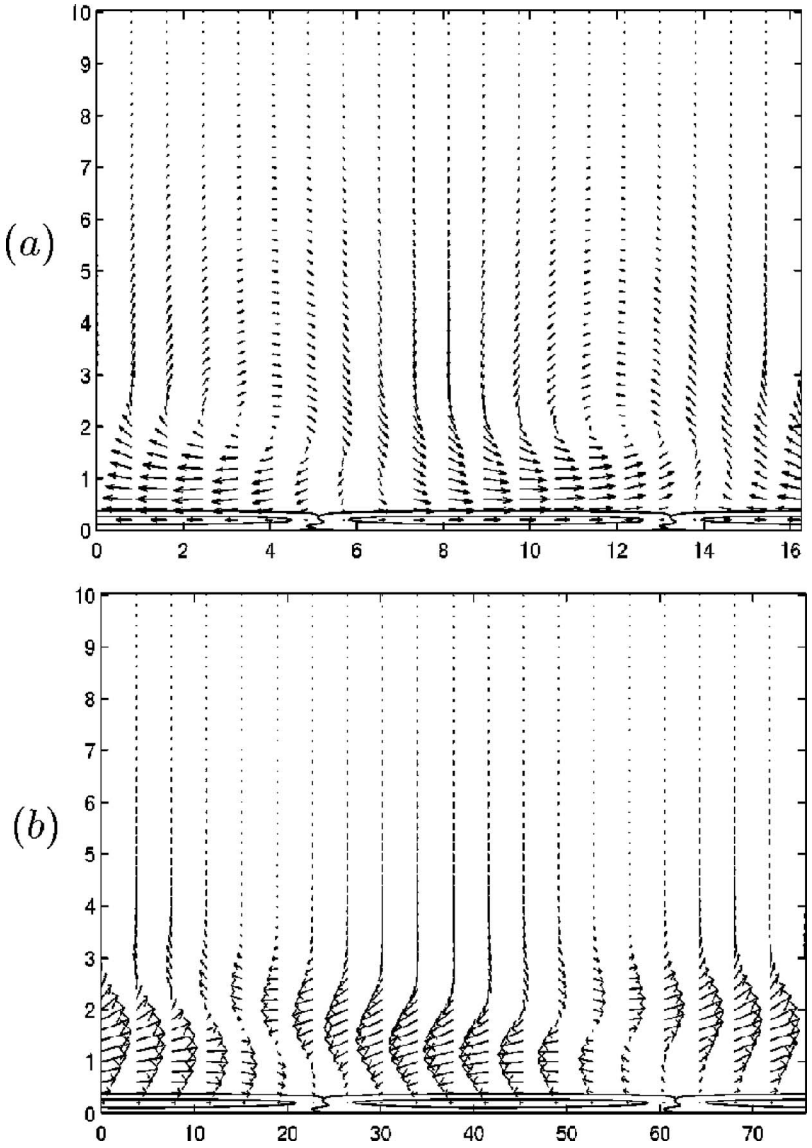

FIG. 9. Reconstruction of the local streamlines at approximately the upper minimum of the neutral curve of hydrodynamic modes ($R=208.77$, $\alpha=0.50869$, and $\beta=0.10206$). The figure shows a plot of the (v_r, v_z) vector in the $R\times z$ plane (a) and a plot of (v_θ, v_z) in the $\theta\times z$ plane (b). Two level curves of the concentration mode c are also shown in the lower part of (a) and (b).

unstable region of chemical modes moves to higher Reynolds numbers as $\nu_0/\nu_\infty \to 1$ and eventually disappears, as the condition of constant viscosity fluid is reached. The neutral stability curve for constant viscosity fluids is recovered.

(4) Even small variations in the fluid viscosity at the electrode interface dramatically shift the neutral curve associated with hydrodynamic modes of constant viscosity to lower Reynolds numbers.

(5) The neutral curves evaluated for $\nu_0/\nu_\infty \leq 1.10$ cross the abscissa axis ($\alpha=0$) at finite values of R, with $\beta \neq 0$. The curves also cross the $\beta\times R$ abscissa axis ($\beta=0$) at finite values of R, with $\alpha \neq 0$. The first case indicates the existence of unstable radial perturbations and the second one the existence of growing circular perturbations. None of these cases had been theoretically identified, though they were experimentally observed by Moisy[16] in the case of two counter-rotating disks.

(6) As an example of marginally unstable radial and circular perturbations, we mention the case with $\nu_0/\nu_\infty=1.020$, where the neutral curve crosses the abscissa axis in the $\alpha\times R$ plane at the point ($\alpha=0$, $\beta=-0.006$, $R=623.7$) and at the point ($\alpha=0.006$, $\beta=0$, $R=695.6$) in the $\beta\times R$ plane.

G. Restoration of the stability properties of constant viscosity electrolytes as ν_0/ν_∞ increases

Results presented in Sec. IV F show that the minimum value of the critical Reynolds number is not attained for $\nu_0/\nu_\infty=2.255$, nor is the new unstable region, associated with this case, the largest one. In this section, we show that, upon increasing the value of ν_0/ν_∞ beyond the value 2.255, the new unstable region also collapses and the neutral curve of hydrodynamic modes moves toward the neutral curve of constant viscosity fluids. The results are shown in Figs. 11 and 12: at first, the new region of chemical modes is reduced and collapses for a value of the ratio ν_0/ν_∞ slightly higher than 2.8. Up to this value, the neutral curve of hydrodynamic modes is only marginally modified. By further increasing the ratio ν_0/ν_∞ to 5.0 and, subsequently, to 10.0, the curve of

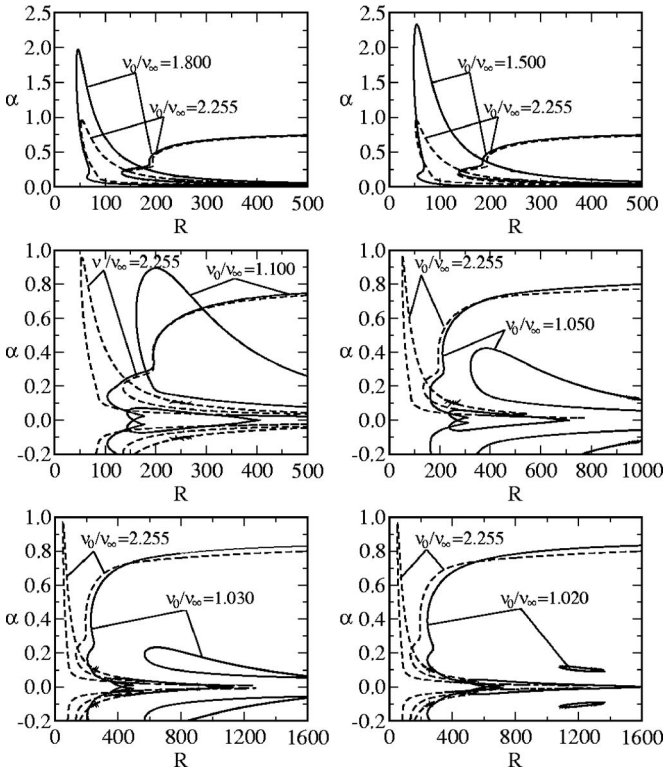

FIG. 10. The collapse of the unstable region of chemical modes as $\nu_0/\nu_\infty \rightarrow 1$, in the plane $\alpha \times R$. Dashed curves refer to $\nu_0/\nu_\infty = 2.255$. Solid lines refer to neutral curves associated with $\nu_0/\nu_\infty = 1.800$ on the top left panel to $\nu_0/\nu_\infty = 1.020$ on the bottom right panel. The curves show that the new unstable region moves to higher Reynolds numbers and eventually disappears as the fluid viscosity approaches a constant value. The most unstable case is not the one for which $\nu_0/\nu_\infty = 2.255$. Similar curves are obtained in the $R \times \beta$ plane.

hydrodynamic modes moves toward the curve of constant viscosity fluids. This result suggests that a progressive increase of the interfacial viscosity and the high Schmidt number leads to an *in facto* discontinuity of the hydrodynamic field, with a thin viscous and stable region at the interface and a restored constant viscosity hydrodynamic boundary layer.

V. CONCLUSIONS

We studied the effect of the coupling of the mass concentration field of one chemical species on the stability of the hydrodynamic field close to an iron rotating disk electrode. The main purpose was to verify whether the current oscillations observed at the beginning of the plateau of the polarization curves, its onset, and collapse could be due to a reduction of the stability of the coupled fields when compared to the stability of the hydrodynamic field of constant viscosity fluids. Since the current is proportional to the normal derivative of the concentration of a relevant chemical species, a sufficiently large instability of the coupled fields at Reynolds numbers attained in experimental conditions can drive detectable current oscillations.

A phenomenological law was assumed, relating the electrolyte viscosity to the concentration of a relevant chemical species originating from the dissolution of the electrode. Parameters in this equation were estimated on the basis of experimental electrochemical data, where the current oscillations were observed.

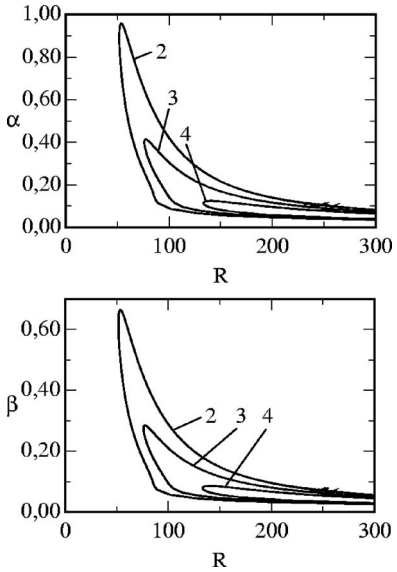

FIG. 11. Collapse of the unstable region of chemical modes as ν_0/ν_∞ increases, shown in the planes $R \times \alpha$ and $R \times \beta$. Curves 2, 3, and 4 refer to $\nu_0/\nu_\infty = 2.255$, 2.5, and 2.8, respectively.

The similarity to von Kármán's solution for rotating disk flow was reevaluated, taking into account the coupling between the hydrodynamic and the mass concentration field. The high bulk Schmidt number of the problem (Sc=2000) leads to a concentration boundary layer having a thickness of the order of 4% of the thickness of the hydrodynamic one. The new velocity profiles are very close to von Kármán's

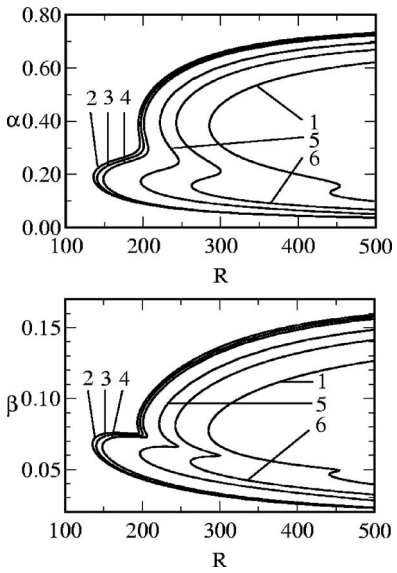

FIG. 12. Effect of the increase of the ratio ν_0/ν_∞ on the neutral curve of hydrodynamic modes. Results presented in the $\alpha \times R$ and $\beta \times R$ planes. This figure shows that the neutral curve of hydrodynamic modes is only slightly affected for values of ν_0/ν_∞ up to 2.8, but tends to the neutral curve of constant viscosity fluids, as ν_0/ν_∞ further increases to 5.0 and to 10.0. Curve 1 refers to the constant viscosity case. Curves 2–6 refer to $\nu_0/\nu_\infty = 2.255$, 2.5, 2.8, 5.0, and 10.0, respectively.

solution, except inside the mass concentration boundary layer, where the profile derivatives are particularly affected and a new inflection in the velocity profiles appears.

A temporal stability analysis of the steady-state solution was performed, with respect to perturbations turning with the angular velocity of the electrode. Small variations introduced in the fluid viscosity by the mass concentration field strongly affect the neutral curve, by enlarging the unstable region, which extends to a broader range of wave numbers and to a critical Reynolds number approximately 50% smaller than the critical one of constant viscosity fluids. In addition, growth rates of unstable modes attain values 30% larger than in the constant viscosity case.

As the viscosity at the interface increases, the stability of the coupled fields is reduced and a new region of unstable modes appears. The overall critical Reynolds number is located in the inner boundary of this region and is close to the experimental values obtained in the electrochemical setup. The critical Reynolds is, in that case, $R=52.3$, a number five times smaller than the critical Reynolds number for constant viscosity fluids, $R=285.36$.

The rate of growth of modes in the new unstable modes is more than one order smaller than the growth rate of modes inside the former unstable region. Nevertheless, the concentration component c of the eigenmodes in the new region is 10 to 20 times larger than the hydrodynamic variables h and η. The eigenfunction is dominated by the concentration, justifying the name of *chemical modes* used for modes in the new unstable region. In addition, the concentration component c is confined to a boundary layer roughly 20 times smaller than the boundary layer of the hydrodynamic variables. The short range in which c varies, together with the large relative value of this variable, leads to large values of $dc/dz|_{z=0}$ and balances the low rate of growth of perturbations in the new unstable region. These perturbations seem, therefore, large enough to drive detectable current oscillations.

The viscosity value at the interface estimated on the basis of experimental electrochemical data, $\nu_0/\nu_\infty=2.255$, does not correspond to the most unstable case. The stability of the coupled fields attains a minimum for a value of the ratio ν_0/ν_∞ close to 1.5. By increasing the viscosity at the interface beyond that value, the stability of the coupled fields tends to that of constant viscosity fluids. At a first moment, the new region of chemical modes is reduced and eventually collapses. The critical Reynolds number moves to values beyond those attained in experimental conditions. Further increases of the viscosity give rise to an *in facto* discontinuity in the coupled fields: a thin high viscosity concentration boundary layer at the interface and a practically constant low viscosity region with restored stability properties: the neutral curve of hydrodynamic modes moves toward the curve of constant viscosity fluids. This mechanism suggests that the suppression of the current oscillations, as the potential applied to electrochemical cell increases, may be due to the sensibility of the new unstable region to the coupled fields, which are progressively divided in a thin viscous region and a practically constant viscosity region. Our group works presently on the kinetics of the anodic dissolution of the electrode, in an effort to understand the mechanism underlying the generation of the chemical species that affects the fluid viscosity, and to reduce the stability of the coupled fields.

ACKNOWLEDGMENTS

The authors acknowledge Professor Alvaro L. G. A. Coutinho and the Center of Parallel Computing (NACAD/COPPE) of the Federal University of Rio de Janeiro, where the numerical calculations were performed. We thank Professor R. E. Kelly from UCLA for fruitful discussions at the beginning of this work. Financial support from the Brazilian agency CNPq is also acknowledged.

APPENDIX A: DERIVATION OF THE BASE STATE EQUATIONS

The equations governing the base state are obtained by assuming that azimuthal derivatives vanish and that the pressure depends on the axial coordinate only. Equations (1)–(3) simplify and take the form

$$\frac{1}{r}\frac{\partial}{\partial r}(rv_r)+\frac{\partial v_z}{\partial z}=0, \tag{A1}$$

$$v_r\frac{\partial v_r}{\partial r}-\frac{v_\theta^2}{r}+v_z\frac{\partial v_r}{\partial z}=2\Omega v_\theta+\Omega^2 r+\frac{1}{\rho}\left(\frac{1}{r}\frac{\partial}{\partial r}(r\tau_{rr})-\frac{\tau_{\theta\theta}}{r}+\frac{\partial \tau_{rz}}{\partial z}\right), \tag{A2}$$

$$v_r\frac{\partial v_\theta}{\partial r}+\frac{v_r v_\theta}{r}+v_z\frac{\partial v_\theta}{\partial z}=-2\Omega v_r+\frac{1}{\rho}\left(\frac{1}{r^2}\frac{\partial}{\partial r}(r^2\tau_{r\theta})+\frac{\partial \tau_{\theta z}}{\partial z}\right), \tag{A3}$$

$$v_z\frac{\partial v_z}{\partial z}=-\frac{1}{\rho}\frac{\partial p}{\partial z}+\frac{1}{\rho}\left(\frac{1}{r}\frac{\partial}{\partial r}(r\tau_{rz})+\frac{\partial \tau_{zz}}{\partial z}\right), \tag{A4}$$

$$v_r\frac{\partial \mathcal{C}}{\partial r}+v_z\frac{\partial \mathcal{C}}{\partial z}=\frac{1}{r}\frac{\partial}{\partial r}\left(\mathcal{D}r\frac{\partial \mathcal{C}}{\partial r}\right)+\frac{\partial}{\partial z}\left(\mathcal{D}\frac{\partial \mathcal{C}}{\partial z}\right). \tag{A5}$$

Upon introducing the constitutive equations of the stress tensor given by Eqs. (4)–(9) in Eqs. (A1)–(A5), we obtain

$$\frac{\partial v_r}{\partial r}+\frac{v_r}{r}+\frac{\partial v_z}{\partial z}=0, \tag{A6}$$

$$v_r\frac{\partial v_r}{\partial r}-\frac{v_\theta^2}{r}+v_z\frac{\partial v_r}{\partial z}=2\Omega v_\theta+\Omega^2 r+\nu\left[\frac{2}{r}\frac{\partial}{\partial r}\left(r\frac{\partial v_r}{\partial r}\right)-\frac{2v_r}{r^2}\right]+\frac{\partial}{\partial z}\left(\nu\frac{\partial v_r}{\partial z}\right), \tag{A7}$$

$$v_r\frac{\partial v_\theta}{\partial r}+\frac{v_r v_\theta}{r}+v_z\frac{\partial v_\theta}{\partial z}=-2\Omega v_r+\frac{\nu}{r^2}\frac{\partial}{\partial r}\left[r^3\frac{\partial}{\partial r}\left(\frac{v_\theta}{r}\right)\right]+\frac{\partial}{\partial z}\left(\nu\frac{\partial v_\theta}{\partial z}\right), \tag{A8}$$

$$v_r\frac{\partial v_z}{\partial r}+v_z\frac{\partial v_z}{\partial z}=-\frac{1}{\rho}\frac{\partial p}{\partial z}+\nu\left[\frac{1}{r}\frac{\partial}{\partial r}\left(r\frac{\partial v_r}{\partial z}\right)+2\frac{\partial^2 v_z}{\partial z^2}\right]+2\frac{\partial \nu}{\partial z}\frac{\partial v_z}{\partial z}, \tag{A9}$$

$$v_z\frac{\partial \mathcal{C}}{\partial z}=\frac{\partial \mathcal{D}}{\partial z}\frac{\partial \mathcal{C}}{\partial z}+\mathcal{D}\frac{\partial^2 \mathcal{C}}{\partial z^2}. \tag{A10}$$

Equations (18), (13), and (12) are introduced in Eqs. (A6)–(A10), leading to the ordinary nonlinear system for the axial profiles F, G, H, P, and C [Eqs. (19)–(23)].

APPENDIX B: THE EVOLUTION EQUATIONS OF THE PERTURBED FLOW

This appendix presents the technical details related to the derivation of the eigenvalue-eigenfunction problem given by Eq. (31). The constitutive equations of the stress tensor, Eqs. (4)–(9), are introduced in nondimensional form, together with the nondimensional Stokes-Einstein and the constitutive equation relating the fluid viscosity to the concentration of the chemical species, Eqs. (13), in the evolution equations [Eqs. (15)–(17)]. Subsequently, the perturbed variables and the base state, given by Eqs. (27) and (29), are introduced in the resulting equations, nonlinear terms are dropped, leading to

$$\frac{\tilde{v}_r}{r}+\frac{\partial \tilde{v}_r}{\partial r}+\frac{1}{r}\frac{\partial \tilde{v}_\theta}{\partial \theta}+\frac{\partial \tilde{v}_z}{\partial z}=0, \tag{B1}$$

$$\begin{aligned}&\frac{\partial \tilde{v}_r}{\partial t}+\frac{r}{R}F\frac{\partial \tilde{v}_r}{\partial r}+\frac{G}{R}\frac{\partial \tilde{v}_r}{\partial \theta}+\frac{H}{R}\frac{\partial \tilde{v}_r}{\partial z}+\frac{F}{R}\tilde{v}_r-\frac{2}{R}(G+1)\tilde{v}_\theta+\frac{r}{R}F'\tilde{v}_z\\&=-\frac{\partial \tilde{p}}{\partial r}+\frac{\bar{\nu}}{R}\left(\frac{\partial^2 \tilde{v}_r}{\partial r^2}+\frac{1}{r^2}\frac{\partial^2 \tilde{v}_r}{\partial \theta^2}+\frac{\partial^2 \tilde{v}_r}{\partial z^2}+\frac{1}{r}\frac{\partial \tilde{v}_r}{\partial r}-\frac{2}{r^2}\frac{\partial \tilde{v}_\theta}{\partial \theta}-\frac{\tilde{v}_r}{r^2}\right)+\frac{\bar{\nu}'}{R}\left(\frac{\partial \tilde{v}_z}{\partial r}+\frac{\partial \tilde{v}_r}{\partial z}\right)+\tilde{\nu}\frac{r}{R}F''\\&\quad+2\frac{F}{R}\frac{\partial \tilde{\nu}}{\partial r}+\frac{r}{R}F'\frac{\partial \bar{\nu}}{\partial z},\end{aligned} \tag{B2}$$

$$\begin{aligned}&\frac{\partial \tilde{v}_\theta}{\partial t}+\frac{r}{R}F\frac{\partial \tilde{v}_\theta}{\partial r}+\frac{G}{R}\frac{\partial \tilde{v}_\theta}{\partial \theta}+\frac{H}{R}\frac{\partial \tilde{v}_\theta}{\partial z}+\frac{F}{R}\tilde{v}_\theta+\frac{2}{R}(G+1)\tilde{v}_r+\frac{r}{R}G'\tilde{v}_z\\&=-\frac{1}{r}\frac{\partial \tilde{p}}{\partial \theta}+\frac{\bar{\nu}}{R}\left(\frac{\partial^2 \tilde{v}_\theta}{\partial r^2}+\frac{1}{r^2}\frac{\partial^2 \tilde{v}_\theta}{\partial \theta^2}+\frac{\partial^2 \tilde{v}_\theta}{\partial z^2}+\frac{1}{r}\frac{\partial \tilde{v}_\theta}{\partial r}+\frac{2}{r^2}\frac{\partial \tilde{v}_r}{\partial \theta}-\frac{\tilde{v}_\theta}{r^2}\right)+\frac{\bar{\nu}'}{R}\left(\frac{1}{r}\frac{\partial \tilde{v}_z}{\partial \theta}+\frac{\partial \tilde{v}_\theta}{\partial z}\right)\\&\quad+\frac{r}{R}G''\tilde{\nu}+\frac{2F}{rR}\frac{\partial \tilde{\nu}}{\partial \theta}+\frac{r}{R}G'\frac{\partial \bar{\nu}}{\partial z},\end{aligned} \tag{B3}$$

$$\begin{aligned}&\frac{\partial \tilde{v}_z}{\partial t}+\frac{r}{R}F\frac{\partial \tilde{v}_z}{\partial r}+\frac{G}{R}\frac{\partial \tilde{v}_z}{\partial \theta}+\frac{H}{R}\frac{\partial \tilde{v}_z}{\partial z}+\frac{H}{R}\tilde{v}_z\\&=-\frac{\partial \tilde{p}}{\partial z}+\frac{\bar{\nu}}{R}\left(\frac{\partial^2 \tilde{v}_z}{\partial r^2}+\frac{1}{r^2}\frac{\partial^2 \tilde{v}_z}{\partial \theta^2}+\frac{\partial^2 \tilde{v}_z}{\partial z^2}+\frac{1}{r}\frac{\partial \tilde{v}_z}{\partial r}\right)\\&\quad+2\frac{\bar{\nu}'}{R}\frac{\partial \tilde{v}_z}{\partial z}+\frac{H''}{R}\tilde{\nu}+\frac{r}{R}F'\frac{\partial \tilde{\nu}}{\partial r}+\frac{G'}{R}\frac{\partial \tilde{\nu}}{\partial \theta}+\frac{2}{R}H'\frac{\partial \tilde{\nu}}{\partial z},\end{aligned} \tag{B4}$$

$$\begin{aligned}&\frac{\partial \tilde{c}}{\partial t}+\frac{r}{R}F\frac{\partial \tilde{c}}{\partial r}+\frac{G}{R}\frac{\partial \tilde{c}}{\partial \theta}+\frac{H}{R}\frac{\partial \tilde{c}}{\partial z}+\tilde{v}_z\frac{dc}{dz}\\&=\frac{1}{RSc}\left\{\bar{\mathcal{D}}\left[\frac{1}{r}\frac{\partial}{\partial r}\left(r\frac{\partial \tilde{c}}{\partial r}\right)+\frac{1}{r}\frac{\partial}{\partial \theta}\left(\frac{1}{r}\frac{\partial \tilde{c}}{\partial \theta}\right)+\frac{\partial^2 \tilde{c}}{\partial z^2}\right]+\frac{d\bar{\mathcal{D}}}{dz}\frac{\partial \tilde{c}}{\partial z}+\tilde{\mathcal{D}}\frac{d^2 c}{dz^2}+\frac{\partial \tilde{\mathcal{D}}}{\partial z}\frac{dc}{dz}\right\}.\end{aligned} \tag{B5}$$

Assuming a perturbation given by Eq. (30) and introducing that form together with Eqs. (14) and (24) in Eqs. (B1)–(B5). we obtain

$$i\left(\alpha-\frac{i}{r}\right)f+i\frac{R}{r}\beta g+h'=0, \tag{B6}$$

$$\begin{aligned}&i\left(\frac{r}{R}\alpha F+\beta G-\omega\right)f+\frac{r}{R}F'h+i\alpha\pi-\frac{r}{R}(F'\gamma c'+F'\gamma' c+F''\gamma c)\\&=\frac{1}{R}\left[\nu f''-\nu\left(\alpha^2+\frac{R^2}{r^2}\beta^2\right)f-Ff+2(G+1)g-Hf'+i\alpha\nu' h+\nu' f'+2i\alpha F\gamma c\right]\\&\quad+\frac{1}{R^2}\left(i\frac{R}{r}\nu\alpha f-2i\frac{R^2}{r^2}\nu\beta g\right)-\frac{\nu}{Rr^2}f,\end{aligned} \tag{B7}$$

$$\begin{aligned}&i\left(\frac{r}{R}\alpha F+\beta G-\omega\right)g+\frac{r}{R}G'h+i\frac{R}{r}\beta\pi-\frac{r}{R}(G''\gamma c+G'\gamma' c+G'\gamma c')\\&=\frac{1}{R}\left[\nu g''-\nu\left(\alpha^2+\frac{R^2}{r^2}\beta^2\right)g-Fg-2(G+1)f-Hg'+i\frac{R}{r}\beta\nu' h+\nu' g'+\frac{2R}{r}i\beta F\gamma c\right]\\&\quad+\frac{1}{R^2}\left(i\frac{R}{r}\nu\alpha g-2i\frac{R^2}{r^2}\nu\beta f\right)-\frac{\nu}{Rr^2}g,\end{aligned} \tag{B8}$$

$$i\left(\frac{r}{R}\alpha F+\beta G-\omega\right)h+\pi'-i\beta G'\gamma c-\frac{r}{R}i\alpha F'\gamma c$$
$$=\frac{1}{R}\left[\nu h''-\nu\left(\alpha^2+\frac{R^2}{r^2}\beta^2\right)h-Hh'-H'h+2\nu'h'+H''\gamma c+2H'\gamma' c+2H'\gamma c'\right]+\frac{i}{Rr}\nu\alpha h, \quad \text{(B9)}$$

$$i\left(\frac{r}{R}\alpha F+\beta G-\omega\right)c+C'h$$
$$=\frac{1}{R\mathrm{Sc}\bar{\nu}}\left\{-\left(\alpha\bar{\alpha}+\frac{R^2}{r^2}\beta^2\right)c+\frac{1}{\bar{\nu}}\left[\left(2\frac{\bar{\nu}'}{\bar{\nu}}\gamma-\gamma'\right)C'-\gamma C''\right]c-\left(\frac{\bar{\nu}'}{\bar{\nu}}+\frac{1}{\bar{\nu}}C'\gamma+\mathrm{Sc}\bar{\nu}H\right)c'+c''\right\}. \quad \text{(B10)}$$

Equations (B6)–(B10) show that perturbation variables are not, strictly speaking, separable. In order to overcome the problem, it is necessary to introduce the *parallel flow* assumption by replacing r by R in Eqs. (B6)–(B10),

$$i\left(\alpha-\frac{i}{R}\right)f+i\beta g+h'=0, \quad \text{(B11)}$$

$$i(\alpha F+\beta G-\omega)f+F'h+i\alpha\pi-(F'\gamma c'+F'\gamma' c+F''\gamma c)$$
$$=\frac{1}{R}[\nu f''-\nu\lambda^2 f-Ff+2(G+1)g-Hf'+i\alpha\nu' h+\nu' f'+2i\alpha F\gamma c]+\frac{1}{R^2}(i\nu\alpha f-2i\nu\beta g)-\frac{\nu}{R^3}f, \quad \text{(B12)}$$

$$i(\alpha F+\beta G-\omega)g+G'h+i\beta\pi-(G''\gamma c+G'\gamma' c+G'\gamma c')$$
$$=\frac{1}{R}[\nu g''-\nu\lambda^2 g-Fg-2(G+1)f-Hg'+i\beta\nu' h+\nu' g'+2i\beta F\gamma c]+\frac{1}{R^2}(i\nu\alpha g-2i\nu\beta f)-\frac{\nu}{R^3}g, \quad \text{(B13)}$$

$$i(\alpha F+\beta G-\omega)h+\pi'-i(\alpha F'+\beta G')\gamma c$$
$$=\frac{1}{R}(\nu h''-\nu\lambda^2 h-Hh'-H'h+2\nu' h'+H''\gamma c+2H'\gamma' c+2H'\gamma c')+\frac{i}{R^2}\nu\alpha h, \quad \text{(B14)}$$

$$i(\alpha F+\beta G-\omega)c+hC'$$
$$=\frac{1}{R\mathrm{Sc}\bar{\nu}}\left\{-\bar{\lambda}^2 c+\frac{1}{\bar{\nu}}\left[\left(2\frac{\bar{\nu}'}{\bar{\nu}}\gamma-\gamma'\right)C'-\gamma C''\right]c-\left(\frac{\bar{\nu}'}{\bar{\nu}}+\frac{1}{\bar{\nu}}C'\gamma+\mathrm{Sc}\bar{\nu}H\right)c'+c''\right\}. \quad \text{(B15)}$$

By eliminating π, neglecting terms of order R^{-2} and smaller, we obtain a system of order 8 of three coupled equations, in the form

$$[i\nu(D^2-\lambda^2)(D^2-\bar{\lambda}^2)+i\nu' D(2D^2-\lambda^2-\bar{\lambda}^2)+i\nu''(D^2+\bar{\lambda}^2)+R(\alpha F+\beta G-\omega)(D^2-\bar{\lambda}^2)-R(\bar{\alpha}F''+\beta G'')-iHD(D^2-\bar{\lambda}^2)$$
$$-iH'(D^2-\bar{\lambda}^2)-iFD^2]h+[2(G+1)D+2G']\eta+\{R(\bar{\alpha}F'+\beta G')\gamma D^2$$
$$+[2R(\bar{\alpha}F''+\beta G'')\gamma+6i\bar{\lambda}^2F\gamma+2R(\bar{\alpha}F'+\beta G')\gamma']D+[R\bar{\lambda}^2(\alpha F'+\beta G')+R(\bar{\alpha}F'''+\beta G''')+4i\bar{\lambda}^2F']\gamma$$
$$+[2R(\bar{\alpha}F''+\beta G'')+6i\bar{\lambda}^2F]\gamma'+R(\bar{\alpha}F'+\beta G')\gamma''\}c=0, \quad \text{(B16)}$$

$$[2(G+1)D-iR(\alpha G'-\beta F')]h+[i\nu(D^2-\lambda^2)+i\nu' D+R(\alpha F+\beta G-\omega)-iHD-iF]\eta$$
$$+[iR(\alpha G'-\beta F')\gamma D+iR(\alpha G''-\beta F'')\gamma+iR(\alpha G'-\beta F')\gamma']c=0, \quad \text{(B17)}$$

$$iR\mathrm{Sc}(\alpha F+\beta G-\omega)c+R\mathrm{Sc}C'h-\frac{1}{\bar{\nu}}\left\{-\bar{\lambda}^2+\frac{1}{\bar{\nu}}\left[\left(2\frac{\bar{\nu}'}{\bar{\nu}}\gamma-\gamma'\right)C'-\gamma C''\right]c-\left(\frac{\bar{\nu}'}{\bar{\nu}}+\frac{1}{\bar{\nu}}C'\gamma+\mathrm{Sc}\bar{\nu}H\right)c'+c''\right\}=0. \quad \text{(B18)}$$

Rearranging of terms of Eqs. (B16)–(B18) leads to Eq. (31).

APPENDIX C: THE NUMERICAL PROCEDURE FOR SOLVING THE STABILITY PROBLEM

Building the neutral curves requires finding the set of points $c(s)=(\alpha(s),\beta(s),R(s))$ that satisfy $F(c(s))=0$, where $F:R^3->R^2$ is given by $F=(\Im(\omega),\Re(\omega)-\omega_r)^T$. The neutral curves are built using a predictor-corrector continuation method described in Ref. 18. Here, for completeness, we will give a short description of the employed method:

(1) The perturbation frequency ω_r is specified, and an initial point, c_0, in the parameters space, α,β,R, is given. This point is not necessarily on the neutral curve.
(2) This initial point is corrected using an inexact Newton iteration given by

$$c_i^{n+1} = c_i^n - F'(c_i^0)^+ F(c_i^n), \tag{C1}$$

where $F'(v_0)^+$ is the pseudoinverse of Moore–Penrose of the Jacobian of F. The Jacobian is computed numerically, using a finite-difference approximation.
(3) To obtain an initial estimate of the next point over the curve, a Predictor step is employed, based on the first-order Euler method:

$$c_{i+1}^0 = c_i + ht[F'(c_i)], \tag{C2}$$

where h is a suitable step size, and $t[F'(c_i)]$ is the tangent vector to curve $c(s)$.
(4) The value c_{i+1}^0 is corrected in a Corrector step using Eq. (C1) iteratively until a satisfactorily converged value is obtained.
(5) The generalized eigenvalue/eigenfunction problem required to evaluate $F(c(s))$ is solved numerically, using an inverse power method double precision routine for complex generalized nonsymmetric eigenproblems, that takes advantage of the sparsity of the coefficient matrices.

[1] V. G. Levich, *Physicochemical Hydrodynamics* (Prentice Hall, Englewood Cliffs, NJ, 1962).
[2] O. E. Barcia, O. R. Mattos, and B. Tribollet, "Anodic dissolution of iron in acid sulfate under mass transport control," J. Electrochem. Soc. **139**, 446 (1992).
[3] A. B. Geraldo, O. E. Barcia, O. R. Mattos, F. Huet, and B. Tribollet, "New results concerning the oscillations observed for the system iron–sulphuric acid," Electrochim. Acta **44**, 455 (1998).
[4] J. Pontes, N. Mangiavacchi, A. R. Conceição, O. E. Barcia, O. E. Mattos, and B. Tribollet, "Rotating disk flow stability in electrochemical cells: Effect of viscosity stratification," Phys. Fluids **16**, 707 (2004).
[5] P. Huerre and P. A. Monkewitz, "Absolute and convective instabilities in free shear layers," J. Fluid Mech. **159**, 151 (1985).
[6] H. Schlichting and K. Gersten, *Boundary Layer Theory* (Springer, Berlin, 1999).
[7] M. R. Malik, "The neutral curve for stationary disturbances in rotating-disk flow," J. Fluid Mech. **164**, 275 (1986).
[8] M. R. Malik, S. Wilkinson, and S. A. Orzag, "Instability and transition in a rotating disk," AIAA J. **19**, 1131 (1981).
[9] S. Wilkinson and M. R. Malik, "Stability experiments in the flow over a rotating disk," AIAA J. **23**, 588 (1985).
[10] R. J. Lingwood, "Absolute instability of the boundary layer on a rotating disk," J. Fluid Mech. **299**, 17 (1995).
[11] P. G. Drazin and W. H. Reid, *Hydrodynamic Stability* (Cambridge, London, 1981).
[12] V. Chikkadi, A. Sameen, and R. Govindarajan, "Preventing transition to turbulence: A viscosity stratification does not always help," Phys. Rev. Lett. **95**, 264504 (2005).
[13] R. Govindarajan, V. L'vov, I. Proaccia, and A. Sameen, "Stabilization of hydrodynamic flows by small viscosity variations," Phys. Rev. E **67**, 026310 (2003).
[14] J. F. Hoburg and J. R. Melcher, "Electrohydrodynamic mixing and instability induced by co-linear fields and conductivity gradients," Phys. Fluids **20**, 903 (1977).
[15] S. V. Malik and A. P. Hooper, "Linear stability and growth of viscosity stratified flows," Phys. Fluids **17**, 024101 (2005).
[16] F. Moisy, O. Doaré, T. Passuto, O. Daube, and M. Rabaud, "Experimental and numerical study of the shear layer instability between two counter-rotating disks," J. Fluid Mech. **507**, 175 (2004).
[17] G. Nicolis, *Introduction to Nonlinear Science* (Cambridge, London, 1995).
[18] E. Allgower and K. Georg, *Continuation Methods—An Introduction* (Springer-Verlag, New York, 1990).